Research Article | Vol. 30, No. 13 / 20 Jun 2022 / Optics Express 22779
Optics EXPRESS

On-chip mode division (de)multiplexer for multi-band operation

QIANSHI WANG,* YU HE, HONGWEI WANG, ZHEN WANG, JIAN SHEN, YONG ZHANG, AND YIKAI SU

State Key Lab of Advanced Optical Communication Systems and Networks, Department of Electronic Engineering, Shanghai Jiao Tong University, Shanghai 200240, China
sjtuwqs@sjtu.edu.cn

Abstract: We propose an on-chip mode division (de)multiplexer based on asymmetric directional couplers (ADCs) for multi-band operation. In mode-coupling process, the minimum coupling length is wavelength-dependent. The longer the wavelength is, the shorter the minimum coupling length is. A light of longer wavelength can be coupled back and forth multiple times with a total coupling length which equals to the minimum coupling length of a shorter wavelength light, thus realizing multi-band transmission at different wavelengths. As a proof-of-concept experiment, a four-mode (de)multiplexer for joint operation in the C- and O-Bands is designed and experimentally demonstrated. For the four modes (TE_0, TE_1, TE_2 and TE_3), the measured insertion losses (ILs) and crosstalk (CT) of the (de)multiplexer are < 4.7 dB and < -10.1 dB respectively from 1290 nm to 1360 nm, and they are < 3.5 dB and < -11.8 dB respectively from 1510 nm to 1580 nm.

1. Introduction

Driven by the exponential growth of the data traffic, it is highly desired to further scale the transmission capacity of photonic integrated circuits (PICs) by employing multiplexing technologies, such as wavelength division multiplexing (WDM) [1,2], mode division multiplexing (MDM) [3–7] and polarization division multiplexing (PDM) [8]. WDM is the most widely used multiplexing technology, while it needs precise wavelength calibration. Recently, as a promising approach, MDM has attracted great interest and it is capable of scaling the transmission capacity by employing orthogonal modes to multiplex optical signals. In addition, MDM technology can be combined with WDM for capacity scaling [9–14].

Mode (de)multiplexers are the key components for MDM systems on silicon-on-insulator (SOI) platforms [15,16]. There are various approaches to achieve on-chip MDM, such as asymmetric directional couplers (ADCs) [17–20], multimode interference (MMI) couplers [21–24] and Y-junctions [25–27]. Mode (de)multiplexers based on MMIs and Y-junctions have broad operation bandwidths and good fabrication tolerances, while the scalabilities of the devices are limited [24,27]. On the other hand, mode (de)multiplexers based on the ADC architecture can achieve high-order mode multiplexing, while the bandwidths are limited due to the stringent phase matching conditions.

Efforts have been put to realize broadband mode (de)multiplexers with good scalabilities. Researchers have successfully achieved a wide operation bandwidth over 100 nm by using a tapered adiabatic directional coupler [17,18]. In addition, a subwavelength waveguide-based ADC is demonstrated with a wide bandwidth of 120 nm due to the reduced confinement of the field and dispersion [19]. These works effectively scale the bandwidth of the ADC-based mode (de)multiplexer. However, most of these ADCs work exclusively on single wavelength band and fail to operate at two or more widely separated bands, which limit their applications towards future multi-band optical systems. For instance, in passive optical network (PON), upstream wavelength and downstream wavelength usually locate at different wavelength bands to

#461551 https://doi.org/10.1364/OE.461551
Journal © 2022 Received 19 Apr 2022; revised 27 May 2022; accepted 30 May 2022; published 7 Jun 2022

Optics EXPRESS

minimize the cost and avoid dispersion compensation [28]. Thus, it is useful to design a mode (de)multiplexer which can operate at different wavelength bands to increase the channel counts of PON systems. To the best of our knowledge, there was only one report on a dual-band (O- and C-bands) (de)multiplexer with two-mode multiplexing using tapered ADCs [20].

In this paper, we propose an on-chip four-mode (de)multiplexer for multi-band operation based on ADCs. It is shown that if the length of the coupling area of an ADC is properly designed, the ADC can realize high transmission efficiency at multi-bands. The basic principle is illustrated as follows: in mode-coupling process, the minimum coupling length is wavelength-dependent. The longer the wavelength is, the shorter the minimum coupling length is. A light of longer wavelength can be coupled back and forth multiple times with a total coupling length which equals to the minimum coupling length of a shorter-wavelength light, thus realizing multi-band transmission at different wavelengths. As a proof-of-concept experiment, we design and experimentally demonstrate the four-mode (de)multiplexer that can operate at both the C- and O-Bands. The measured insertion losses (ILs) and crosstalk (CT) of the (de)multiplexer are less than 4.7 dB and −10 dB respectively, in the wavelength range from 1290 nm to 1360 nm for TE_0, TE_1, TE_2 and TE_3 modes. Similarly, the ILs and CT of the (de)multiplexer are lower than 3.2 dB and −11.8 dB, respectively, from 1510 nm to 1580 nm for all the four modes.

2. Principle

In coupled-mode theory (CMT), the fundamental mode in the access waveguide can be coupled to a high-order mode in a bus waveguide when the phase matching condition is satisfied, which can be expressed as:

$$n_{TE0\_access} = n_{TEi\_bus}, \tag{1}$$

where n_{TE0_access} and n_{TEi_bus} are the effective refractive indices of the fundamental mode in the access waveguide and the i-th order mode in the bus waveguide, respectively. The effective index of the guided mode is related to the geometry of the waveguide. The thickness of the waveguide is usually fixed to 220 nm for a commercial SOI wafer. For a given width of access waveguide (w_{access} = 350 nm in this case), the dimension of the bus waveguide is fixed in order to satisfy the phase matching condition. However, the effective refractive index of the guided mode varies with the operating wavelength. It means that the width of the bus waveguide needs to be changed when the operating wavelength varies which limits the bandwidth of the ADC. Table 1 shows the calculated bus waveguide widths for different modes to couple with a 350-nm-width access waveguide at λ_1 = 1310 nm and λ_2 = 1550 nm, respectively. It can be noted that the optimal waveguide widths for the two wavelengths are different but the deviation is minor. We set the width of the bus waveguide between the optimal widths for 1310 nm and 1550 nm. Thus, the designed ADC can realize the mode coupling at both wavelengths at the cost of an acceptable performance degradation.

Table 1. Calculated optimal widths (nm) of the bus waveguide for TE_1~TE_4 modes[a]

	TE_1	TE_2	TE_3	TE_4
1310 nm	740	1130	1520	1900
1550 nm	723	1100	1480	1830

[a]The access waveguide is set to 350 nm. The results are simulated by Lumerical MODE solutions.

The coupling length is the main factor that affects the operation bandwidth of the ADC. In CMT, the mode coupling can be a periodic phenomenon which means that the light will be periodically coupled back and forth between the access waveguide and the bus waveguide. The

Optics EXPRESS

optimal coupling length L_c is not unique which is denoted by [29]:

$$L_c = (2m + 1)L_0 \tag{2}$$

$$L_0 = \frac{\pi}{2\kappa_{ab}} \tag{3}$$

$$\kappa_{ab} = \frac{\omega\varepsilon_0}{4}\iint (n_{core}^2 - n_{clad}^2)E_{ay}^*(x,y)E_{by}(x,y)dxdy, \tag{4}$$

where m is a natural number, L_0 is the minimum coupling length, κ_{ab} is the coupling coefficient, ω is the frequency, ε_0 is the vacuum permittivity, n_{core} and n_{clad} are the refractive indices of the waveguide and the cladding, respectively. E_{ay} and E_{by} are the distributions of the transverse electric mode in the access waveguide and bus waveguide, respectively. The equations show that the coupling length is wavelength-dependent, thus affecting the bandwidth of the ADC.

In a conventional ADC, light is usually coupled from the access waveguide to the bus waveguide in the first period ($m = 0$) to minimize the footprint of the device. If we do not limit the length of the device, it may happen that a light of one wavelength can be coupled from the access waveguide to the bus waveguide with $m = m_1$ and another light of a different wavelength can show different periods ($m = m_2$) over the same total length:

$$L_{c1} = L_{c2} \tag{5}$$

$$(2m_1 + 1)L_{01} = (2m_2 + 1)L_{02}, \tag{6}$$

where L_{c1} and L_{c2} are the total coupling lengths for two different wavelengths, L_{01} and L_{02} are minimum coupling lengths for the two wavelengths, m_1 and m_2 are the numbers of periods. If there are m_1 and m_2 values that satisfy Eq. (5), the designed ADC can operate at two wavelengths, consequently increasing the available operation band of the ADC at the cost of increased length of the device. Using the method, we design a four-mode (de)multiplexer operating at both C- and O-bands as shown in the following.

3. Design and simulation

In this work, we choose $\lambda_1 = 1310$ nm and $\lambda_2 = 1550$ nm as the operating wavelengths because the two wavelengths are widely used in optical communication systems [30]. The structure of the designed ADC for TE_1 mode is illustrated in Fig. 1. The width of the access waveguide is narrower than a conventional single-mode waveguide, which helps to strengthen the coupling and shorten the coupling length [14]. The gap between the access waveguide and the bus waveguide is set to be 100 nm. The widths of the bus waveguide for TE_1, TE_2 and TE_3 modes are set to be 730 nm, 1100 nm and 1500 nm, respectively, referring to Table 1.

Take the design of the ADC for TE_1 mode as an example. The following simulations and optimizations are carried out by Lumerical FDTD solutions. The simulated coupling lengths L_{01} for 1310 nm and L_{02} for 1550 nm are 13.2 μm and 4.9 μm, respectively. If $m_1 = 0$ and $m_2 = 1$, Eq. (5) can be approximately satisfied. In other words, the light at 1550-nm wavelength can be coupled to the bus waveguide during the second period and the light at 1310-nm wavelength can be coupled to the bus waveguide in the first period as shown in Fig. 2(a) and (b). Therefore, the coupling length L_c of the ADC is set to be 13.5 μm. The simulated transmission response of the designed ADC is shown in the Fig. 3(a). We can notice that there are two obvious peaks in the transmission spectrum which prove the feasibility of the ADC for multi-band operation. At $\lambda_1 = 1310$ nm and $\lambda_2 = 1550$ nm, the ILs are 0.35 and 1.02 dB, respectively. Figure 3(a) illustrates that the transmission efficiency is not high and the bandwidth is limited around $\lambda_2 = 1550$ nm because the coupling length L_c is not the optimal for the wavelengths around 1550 nm. In order to further improve the performance, we taper the access waveguide and the bus waveguide and the

Optics EXPRESS

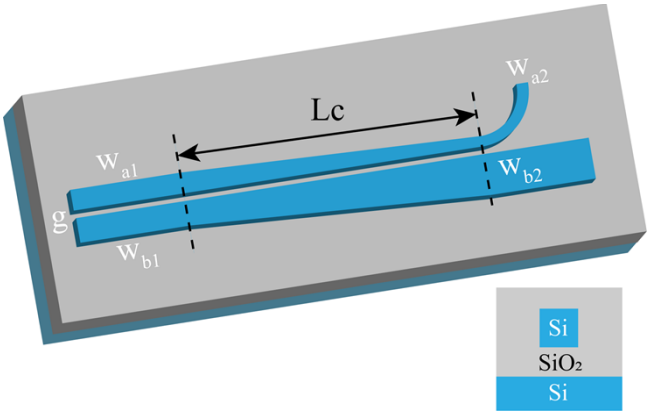

Fig. 1. Structure of the designed ADC for both C- and O-bands

simulated transmission spectrum is shown in Fig. 3(b). At $\lambda_1 = 1310$ nm and $\lambda_2 = 1550$ nm, the ILs are 0.64 and 0.72 dB, respectively. The bandwidth increases greatly around $\lambda_1 = 1310$ nm and $\lambda_2 = 1550$ nm. The light around $\lambda_1 = 1310$ nm cannot be coupled back due to the phase mismatch resulting from the counter-tapered ADC [17], leading to a broader bandwidth. The coupling strength of the light around $\lambda_2 = 1550$ nm is stronger than that of the light around $\lambda_1 = 1310$ nm so the light around $\lambda_2 = 1550$ nm can still be periodically coupled between the waveguides. The counter-tapered ADC can relax the phase matching condition for the light around $\lambda_2 = 1550$ nm and make the light easier to be coupled to the bus waveguide.

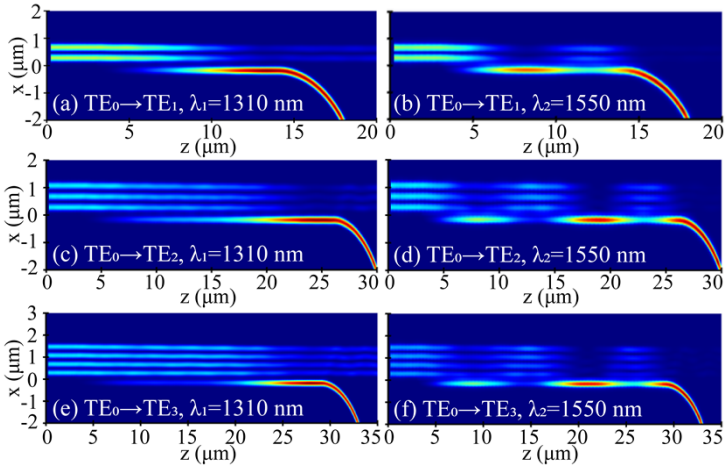

Fig. 2. Simulated power distributions of the counter-tapered ADC for (a) TE_1 mode at $\lambda_1 = 1310$ nm, (b) TE_1 mode at $\lambda_2 = 1550$ nm, (c) TE_2 mode at $\lambda_1 = 1310$ nm, (d) TE_2 mode at $\lambda_2 = 1550$ nm, (e) TE_3 mode at $\lambda_1 = 1310$ nm, (f) TE_3 mode at $\lambda_2 = 1550$ nm.

According to this method, we also design the ADCs for TE_2 and TE_3 modes, respectively. The simulated power distributions of the designed ADCs are shown in Fig. 2 and the simulated transmission spectra are shown in Fig. 3(c) and (d), respectively. The ILs are 0.59 dB and 0.78 dB for TE_2 mode and the ILs are 0.80 dB and 0.75 dB for TE_3 mode at $\lambda_1 = 1310$ nm and $\lambda_2 = 1550$ nm. During the design and simulation process, we find that the transmission around $\lambda_2 = 1550$ nm can be improved by accurately extending the length of the device to the coupling

Optics EXPRESS

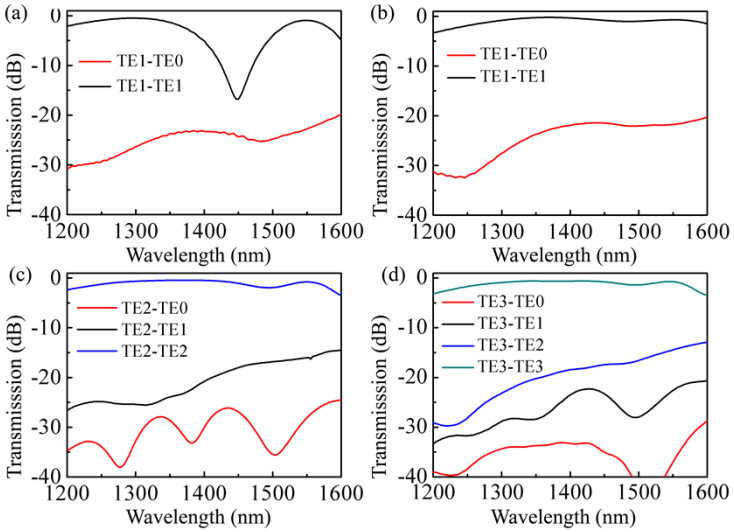

Fig. 3. Simulated transmission spectra of (a) the conventional ADC for TE_1 mode, (b) the designed ADC for TE_1 mode, (c) the designed ADC for TE_2 mode, (d) the designed ADC for TE_3 mode.

length L_c when $m_2 = 2$, which means that the light at 1550-nm wavelength can be coupled to the bus waveguide during the third period, as shown in Fig. 2(d) and (f). And the transmission around $\lambda_1 = 1310$ nm can also be improved by extending the length of the device due to the counter-tapered ADC structure. The parameters of the designed ADCs are shown in Table 2.

Table 2. Parameters of the designed ADCs for TE_1, TE_2 and TE_3 modes

	W_{a1} (nm)	W_{a2} (nm)	W_{b1} (nm)	W_{b2} (nm)	L_c (μm)	Gap (nm)
TE_1	370	330	690	750	13	100
TE_2	370	340	1060	1160	25	100
TE_3	370	340	1440	1560	28	100

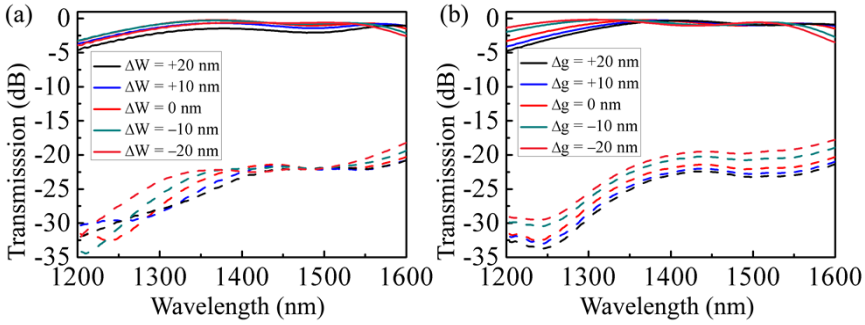

Fig. 4. Simulated transmission spectra of the designed ADCs for TE_1 mode with variations in (a) the access and the bus waveguide widths ΔW and (b) the coupling gap Δg. Dashed lines indicate crosstalk.

To investigate the fabrication-error tolerance of the proposed ADC, transmission spectra of the ADC for TE_1 mode with different waveguide widths and coupling gaps are shown in Fig. 4.

Optics EXPRESS

The simulation results show that the ILs are < 2.33 dB and the CT values are < −19.2 dB in the two wavelength ranges (1290 nm~1360 nm & 1510 nm~1580 nm) with the variation of the waveguide width by ±10 nm and ±20 nm. And the ILs are < 2.62 dB and the CT values are < −18.4 dB in the two wavelength ranges if the coupling gap varies by ±10 nm and ±20 nm. In summary, the proposed ADCs exhibit a good fabrication-error tolerance. Fabrication errors are major challenges for achieving integrated photonic devices with stable performances. While one can mitigate the fabrication variation effects by means of post-fabrication adjustments, such as post-fabrication trimming [31–33] to enhance the performance of the fabricated device.

4. Fabrication and characterization

In the experiment, two identical four-mode (de)multiplexers operating at both C- and O-bands were fabricated on an SOI wafer with a 220-nm silicon layer on top of a 3-μm silica bottom layer. The structures and grating couplers were patterned by e-beam lithography (Vistec EBPG 5200+) and fully etched by inductively coupled plasma (ICP) etching. Then, a 1-μm SiO_2 cladding layer was deposited by plasma-enhanced chemical vapor deposition (PECVD, Oxford). The microscope images and SEM images of the fabricate device are shown in Fig. 5. Due to the limited bandwidths of the grating couplers, we designed identical mode (de)multiplexers on the same chip with O-band and C-band grating couplers, respectively, to characterize the performance of the device. Accordingly, two tunable continuous wave (CW) laser (Keysight 81960A & Santec TSL-550) were used as C-band and O-band light sources, respectively. An optical power meter (Keysight N7744A) was used to characterize the devices.

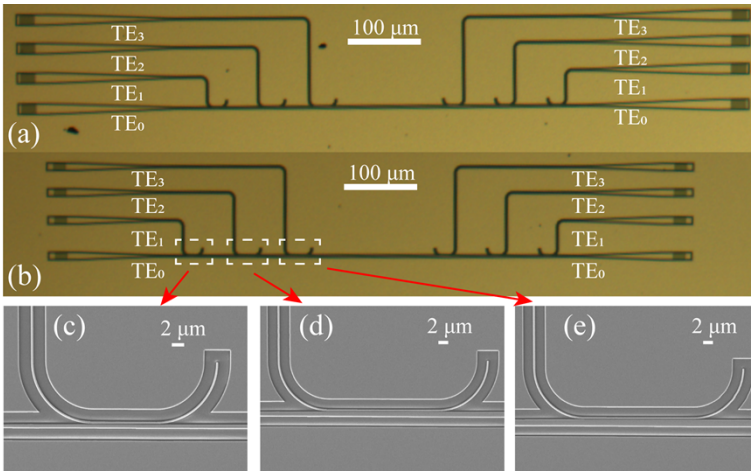

Fig. 5. Microscope images of the four-mode (de)multiplexers with (a) C-band grating couplers and (b) O-band grating couplers, (c)-(e) SEM images of the coupling areas for TE1-TE3, respectively.

Figure 6(a)-(d) show the measured transmission spectra at four output ports (TE_0~TE_3) of the mode (de)multiplexers when the O-band signal is launched from the TE_0, TE_1, TE_2 and TE_3 input ports, respectively. Figure 6(e)-(h) show the measured transmission spectra at four output ports (TE_0~TE_3) of the mode (de)multiplexers when the C-band light is launched from TE_0, TE_1, TE_2 and TE_3 input port, respectively. The measured transmission spectra are normalized to the same grating couplers fabricated on the same wafer. As shown in Fig. 6(a)-(d), the ILs are < 1.2 dB, 3.8 dB, 2.7 dB and 4.7 dB and the CT values are < −15.6 dB, −10.9 dB, −12.0 dB and −10.1 dB in the wavelength range of 1290 nm ~ 1360 nm for TE_0~TE_3 mode channels. As shown in Fig. 6(e)-(h), the ILs are < 0.9 dB, 2.3 dB, 3.5 dB and 3.2 dB and the CT values are <

Optics EXPRESS

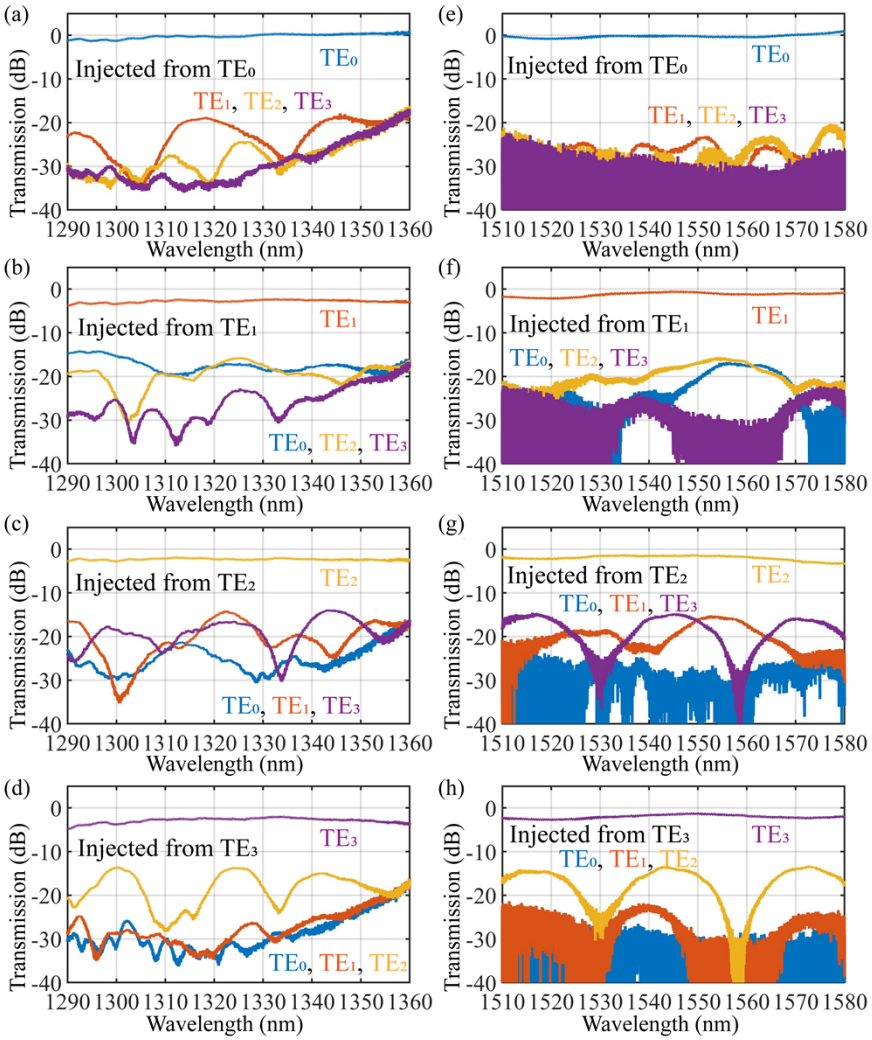

Fig. 6. Measured transmission spectra at the four output ports of the mode demultiplexers when O-band light is launched from input port (a) TE_0, (b) TE_1, (c) TE_2, (d) TE_3 and when C-band light is launched from input port (e) TE_0, (f) TE_1, (g) TE_2, (h) TE_3.

−20.0 dB, −14.7 dB, −12.6 dB and −11.8 dB in the wavelength range of 1510 nm ~ 1580 nm for TE_0~TE_3 mode channels, respectively. In Fig. 3, the simulation results show that the ILs are < 1.01 dB and the CT values are < −19.5 dB from 1290 nm to 1360 nm for all four mode channels. The ILs are < 2.28 dB and the CT values are < −13.4 dB from 1510 nm to 1580 nm for four mode channels, respectively. The measured results are in good agreement with the simulation results in the wavelength range from 1510 nm to 1580 nm. From 1290 nm to 1360 nm, the measured results deteriorate obviously compared with the simulation results which can be contributed to the waveguide dimension deviation caused by fabrication errors.

Finally, Table 3 summarizes the performances of several recently reported four-mode (de)multiplexers. Our proposed structure shows the widest operation bandwidth with reasonable insertion loss, crosstalk, and footprint out of four-mode on-chip (de)multiplexers.

Optics EXPRESS

Table 3. Comparison of the reported four-mode (de)multiplexers

Structure	IL (dB)	CT (dB)	BW (nm)	Length (μm)	Platform	Reference
SWG-assisted TWC	< 5	< −10	100	48.964	SOI	[34]
Tapered ADC	< 1.6	< −16	100	197	LN-SRN	[35]
WFM ADC	< 1.31	< −10	117	239.6	SOI	[36]
SWG ADC	< 4	< −16	50	19.8	SOI	[37]
This work	< 4.7	< −10.1	140	66	SOI	—

5. Conclusion

In conclusion, we proposed and experimentally demonstrated an on-chip mode division (de)multiplexer for multi-band operation. The (de)multiplexer leverages the periodicity of the mode coupling to realize high transmission efficiency at separated bands. In addition, the (de)multiplexer uses the counter-tapered ADC to improve the transmission efficiency and bandwidth. The measured results show that the CT values are below −10.1 dB from 1290 nm to 1360 nm and less than −11.8 dB from 1510 nm to 1580 nm for four mode channels covering C-band, most part of the O-band and small portions of S- and L-bands. The total measured bandwidth of the (de)multiplexer is 140 nm with an IL of < 4.7 dB and a CT of < −10.1 dB. The designed ADC is expected to be further extended to higher orders.

Funding. National Natural Science Foundation of China (61835008, 61860206001).

Acknowledgment. We thank the Center for Advanced Electronic Materials and Devices (AEMD) of Shanghai Jiao Tong University for the support in device fabrications.

Disclosures. The authors declare no conflicts of interest.

Data availability. Data underlying the results presented in this paper are not publicly available at this time but may be obtained from the authors upon reasonable request.

References

1. Q. Fang, T. Liow, J. Song, K. Ang, M. Yu, G. Lo, and D. Kwong, "WDM multi-channel silicon photonic receiver with 320 Gbps data transmission capability," Opt. Express **18**(5), 5106–5113 (2010).
2. Z. Zhang, H. Li, B. J. Huang, Z. Y. Zhang, C. T. Cheng, T. X. Gao, Y. X. Yu, Y. M. Li, and H. D. Chen, "Multi-channel silicon photonic receiver based on compact second-order microring resonators," Opt. Commun. **437**, 168–173 (2019).
3. J. Wang, Y. Xuan, M. Qi, L. Liu, and G. N. Liu, "Ultra-broadband Integrated Four-Channel Mode-Division-Multiplexing Based on Tapered Mode-Evolution Couplers," in *42nd European Conference on Optical Communication (ECOC)* (2016), pp. 1–3.
4. W. Chang, L. Lu, X. Ren, D. Li, Z. Pan, M. Cheng, D. Liu, and M. Zhang, "Ultra-compact mode (de) multiplexer based on subwavelength asymmetric Y-junction," Opt. Express **26**(7), 8162–8170 (2018).
5. Y. He, Y. Zhang, Q. Zhu, S. An, R. Cao, X. Guo, C. Qiu, and Y. Su, "Silicon High-Order Mode (De)Multiplexer on Single Polarization," J. Lightwave Technol. **36**(24), 5746–5753 (2018).
6. H. Xie, Y. Liu, S. Wang, Y. Wang, Y. Yao, Q. Song, J. Du, Z. He, and K. Xu, "Highly compact and efficient four-mode multiplexer based on pixelated waveguides," IEEE Photonics Technol. Lett. **32**(3), 166–169 (2020).
7. C. H. Yao, Z. Wang, H. W. Wang, Y. He, Y. Zhang, and Y. K. Su, "On-Chip Multi-Mode Manipulation via 2D Refractive-Index Perturbation on a Waveguide," Adv. Opt. Mater. **8**(23), 2000996 (2020).
8. D. Dai, C. Li, S. Wang, H. Wu, Y. Shi, Z. Wu, S. Gao, T. Dai, H. Yu, and H. K. Tsang, "10-channel Mode (de) multiplexer with dual polarizations," Laser Photonics Rev. **12**(1), 1700109 (2018).
9. L.-W. Luo, N. Ophir, C. P. Chen, L. H. Gabrielli, C. B. Poitras, K. Bergmen, and M. Lipson, "WDM-compatible mode-division multiplexing on a silicon chip," Nat. Commun. **5**(1), 3069 (2014).
10. D. Dai, J. Wang, S. Chen, S. Wang, and S. He, "Monolithically integrated 64-channel silicon hybrid demultiplexer enabling simultaneous wavelength-and mode-division-multiplexing," Laser Photonics Rev. **9**(3), 339–344 (2015).
11. Z. Chen, Y. Zhu, X. Ruan, Y. Li, Y. Li, and F. Zhang, "Bridged coupler and oval mode converter based silicon mode division (De)multiplexer and terabit WDM-MDM system demonstration," J. Lightwave Technol. **36**(13), 2757–2766 (2018).
12. G.-H. Chen, C.-W. Chow, C.-H. Yeh, C.-W. Peng, P.-C. Guo, J.-F. Tsai, M.-W. Cheng, Y. Tong, and H.K. Tsang, "Mode-division-multiplexing (MDM) of 9.4-Tbit/s OFDM signals on silicon-on-insulator (SOI) platform," IEEE Access **7**, 129104–129111 (2019).

Optics EXPRESS

13. Y. Hsu, C.-Y. Chuang, X. Wu, G.-H. Chen, C.-W. Hsu, Y.-C. Chang, C.-W. Chow, J. Chen, Y.-C. Lai, C.-H. Yeh, and H. K. Tsang, "2.6 Tbit/s on-chip optical interconnect supporting mode-division-multiplexing and PAM-4 signal," IEEE Photonics Technol. Lett. **30**(11), 1052–1055 (2018).
14. G.-H. Chen, J.-F. Tsai, C.-W. Peng, P.-C. Kuo, C.-J. Chen, C.-W. Chow, C.-H. Yeh, Y. Lai, and Y. Liu, "Compact Mode Division MUX/DEMUX Using Enhanced Evanescent-Wave Coupling on Silicon-on-Insulator (SOI) Platform for 11-Tbit/s Broadband Transmission," IEEE Access **8**, 219881–219890 (2020).
15. Y. Su, Y. Zhang, C. Qiu, X. Guo, and L. Sun, "Silicon photonic platform for passive waveguide devices: materials, fabrication, and applications," Adv. Mater. Technol. **5**(8), 1901153 (2020).
16. Y. Su and Y. Zhang, *Passive Silicon Photonic Devices: Design, Fabrication, and Testing* (AIP Publishing, 2022), Chap. 7.
17. Y. Ding, J. Xu, F. Da Ros, B. Huang, H. Ou, and C. Peucheret, "On-chip two-mode division multiplexing using tapered directional coupler-based mode multiplexer and demultiplexer," Opt. Express **21**(8), 10376–10382 (2013).
18. J. Wang, Y. Xuan, M. Qi, H. Huang, Y. Li, M. Li, X. Chen, Z. Sheng, A. Wu, W. Li, X. Wang, S. Zou, and F. Gan, "Broadband and fabrication-tolerant on-chip scalable mode-division multiplexing based on mode-evolution counter-tapered couplers," Opt. Lett. **40**(9), 1956–1959 (2015).
19. Z. Jafari, A. Zarifkar, and M. Miri, "Compact fabrication-tolerant subwavelength-grating-based two-mode division (de)multiplexer," Appl. Opt. **56**(26), 7311–7319 (2017).
20. B. Paredes, Z. Mohammed, J. Villegas, and M. Rasras, "Dual-Band (O & C-Bands) Two-Mode Multiplexer on the SOI Platform," IEEE Photonics J. **13**(3), 1–9 (2021).
21. T. Uematsu, Y. Ishizaka, Y. Kawaguchi, K. Saitoh, and M. Koshiba, "Design of a Compact Two-Mode Multi/Demultiplexer Consisting of Multimode Interference Waveguides and a Wavelength-Insensitive Phase Shifter for Mode-Division Multiplexing Transmission," J. Lightwave Technol. **30**(15), 2421–2426 (2012).
22. L. Han, S. Liang, H. Zhu, L. Qiao, J. Xu, and W. Wang, "Two-mode de/multiplexer based on multimode interference couplers with a tilted joint as phase shifter," Opt. Lett. **40**(4), 518–521 (2015).
23. D. González-Andrade, A. Dias, J. G. Wangüemert-Pérez, A. Ortega-Moñux, Í. Molina-Fernández, R. Halir, P. Cheben, and A. V. Velasco, "Experimental demonstration of a broadband mode converter and multiplexer based on subwavelength grating waveguides," Opt. Laser Technol. **129**, 106297 (2020).
24. Z. Wang, C. Yao, Y. Zhang, and Y. Su, "Compact silicon three-mode multiplexer by refractive-index manipulation on a multi-mode interferometer," Opt. Express **29**(9), 13899–13907 (2021).
25. J. Driscoll, R. Grote, B. Souhan, J. Dadap, M. Lu, and R. Osgood, "Asymmetric Y junctions in silicon waveguides for on-chip mode-division multiplexing," Opt. Lett. **38**(11), 1854–1856 (2013).
26. W. Zhao, J. Feng, K. Chen, and K. Chiang, "Reconfigurable broadband mode (de)multiplexer based on an integrated thermally induced long-period grating and asymmetric Y-junction," Opt. Lett. **43**(9), 2082–2085 (2018).
27. Y. Gao, D. Zhang, Y. Xu, L. Ji, W. Chen, X. Wang, W. Gao, and X. Sun, "Compact six-mode (de)multiplexer based on cascaded asymmetric Y-junctions with mode rotators," Opt. Commun. **451**, 41–45 (2019).
28. J. Wey, "The Outlook for PON Standardization: A Tutorial," J. Lightwave Technol. **38**(1), 31–42 (2020).
29. W. Huang, "Coupled-mode theory for optical waveguides: an overview," J. Opt. Soc. Am. A **11**(3), 963–983 (1994).
30. P. Winzer, D. Neilson, and A. Chraplyvy, "Fiber-optic transmission and networking: the previous 20 and the next 20 years [Invited]," Opt. Express **26**(18), 24190–24239 (2018).
31. S. Grillanda, V. Raghunathan, V. Singh, F. Morichetti, J. Michel, L. Kimerling, A. Melloni, and A. Agarwal, "Post-fabrication trimming of athermal silicon waveguides," Opt. Lett. **38**(24), 5450–5453 (2013).
32. H. Jayatilleka, H. Frish, R. Kumar, J. M. Heck, C. Ma, M. Sakib, D. Huang, and H. Rong, "Post-fabrication trimming of silicon photonic ring resonators at wafer-scale," J. Lightwave Technol. **39**(15), 5083–5088 (2021).
33. R. M. Krishna, A. Eftekhar, S. Lee, T. Fan, X. Wu, A. Hosseinnia, H. Wang, M. Swaminathan, and A. Adibi, "Polysilicon micro-heaters for resonance tuning in CMOS photonics," Opt. Lett. **47**(5), 1097–1100 (2022).
34. W. Jiang, J. Hu, S. Mao, H. Zhang, L. Zhou, and B. M. Azizur Rahman, "Broadband Silicon Four-Mode (De)Multiplexer Using Subwavelength Grating-Assisted Triple-Waveguide Couplers," J. Lightwave Technol. **39**(15), 5042–5047 (2021).
35. Y. Liu, X. Huang, Z. Li, H. Guan, Z. Yu, Q. Wei, Z. Fan, W. Han, and Z. Li, "On-chip four-mode (de-)multiplexer on thin film lithium niobate–silicon rich nitride hybrid platform," Opt. Lett. **46**(13), 3179–3182 (2021).
36. Y. Sawada, T. Fujisawa, T. Sato, and K. Saitoh, "Broadband silicon four-mode multi/demultiplexer designed by a wavefront matching method," Opt. Express **29**(17), 27322–27331 (2021).
37. X. Wang, H. Yu, Q. Zhang, Z. Fu, P. Xia, Q. Huang, N. Ning, Z. Wei, Y. Wang, X. Jiang, and J. Yang, "Ultra-compact silicon mode (de)multiplexer based on directional couplers with subwavelength sidewall corrugations," Opt. Lett. **47**(9), 2198–2201 (2022).